Polaritons in anisotropic materials with cylindrical geometry

E. F. Nobre, R. N. Costa Filho, and G. A. Farias*
Departamento de Física , Universidade Federal do Ceará, Campus do Pici, Cx. P. 6030, CEP 60.451-970 - Fortaleza, CE, Brazil

N. S. Almeida
Departamento de Física Teórica e Experimental, Centro de Ciências Exatas, Universidade Federal do Rio Grande do Norte, CEP 59.072-970 - Natal, RN, Brazil

(Received 19 November 1997)

The properties of polaritons propagating in an anisotropic material with a cylindrical geometry are studied. Solving Maxwell's equations for nonradiative modes, the dispersion relation, power flows, energy densities, and the group velocity of the polaritons are obtained. It is shown that the nonradiative modes can propagate in two different modes namely confined or localized modes. The significative differences between these modes are presented. The uniaxial Heisenberg antiferromagnet MnF_2 is used in order to obtain numerical results. [S0163-1829(98)05517-9]

I. INTRODUCTION

Surface polaritons are a sensitive probe in surface analysis since they can provide valuable information about the parameters associated with the surface. This is a subject that has been studied for many years but the propagation of these coupled modes in different materials and geometries are still the subject of much research.[1–6] Particularly, in magnetic materials, polaritons propagating in antiferromagnetic materials in a planar geometry have been theoretically well studied.[3–6] Recently Jensen *et al.*[7] reported the direct experimental observation of magnetic surface polaritons in an uniaxial antiferromagnet material by using the attenuated total reflection technique.

Most of the studies of these collective modes are restricted to geometry where the surfaces are flat planes or spheres. It is well known that the planar, as well as the spherical geometry, always allow pure magnetic waves (TM modes) and pure electric waves (TE modes) as the two independent solutions of the Maxwell's equations. This is not the case when the surfaces are cylindrical. In this later geometry the separation of TE and TM modes is allowed only in particular cases. This fact makes the problem a rather complicated one. However, the cylindrical geometry is quite attractive since it is an intermediate geometry and then it should exhibit characteristics of the two others. Moreover, this geometry is a good candidate to be used in experiments and could better reveal properties of surfaces as well as of materials. It should be mentioned that objects with cylindrical geometry have been proposed as an important tool to study the scattering of electromagnetic waves by surfaces.[8,9]

The physical behavior of electromagnetic waves propagating in cylinders of isotropic nonmagnetic material has been well known for many years.[10–12] However, similar study for anisotropic materials has received little attention. Recently, Vasconcelos *et al.*[13] studied polaritons propagating in a cylinder with uniaxial anisotropy and obtained the dispersion relation of nonradiative polaritons confined in an uniaxial anisotropic antiferromagnetic material. They also found solutions similar to those obtained for isotropic cylinders,[10] i.e., in these anisotropic materials the solutions also have TE and TM modes coupled together, unless they are modes with no angular dependence. Shortly after, Almeida *et al.*[14] showed that the presence of an external static magnetic field applied parallel to the axis of the uniaxial anisotropy and parallel to the cylinder axis can decouple these modes. They found an implicit dispersion relation and, from that, they obtained theoretical dispersion curves for surface and bulk modes confined into an uniaxial Heisenberg antiferromagnetic specimen. The main motivation for the study of mixed modes in cylindrical geometry is the possibility of using it for practical purposes (optical fibers, for example). Therefore, besides dispersion relation curves, it is necessary to know the electromagnetic field distribution as well as how the energy is transported in the material.

In the present paper, we generalize the work of Vasconcelos *et al.*[13] by studying the electromagnetic field distribution and energy transport of the nonradiative confined and localized polaritons propagating in an uniaxial anisotropic material with a cylindrical geometry. To do this, we solve the Maxwell's equations in order to calculate the electric and magnetic fields inside and outside the cylinder. Using the boundary conditions at the cylinder interface we obtain an implicit dispersion relation of volume and surface modes, power flows, energy densities of electromagnetic field, and the group velocity of the polaritons. In the last section we present the numerical results obtained considering the uniaxial Heisenberg antiferromagnet MnF_2.

II. MODEL

The system under consideration is a long cylinder of radius $r=a$ with its axis parallel to the anisotropy direction and immersed in an isotropic medium which, without loss of generality, we will consider to be the vacuum. The cylinder is characterized by the dielectric ($\overleftrightarrow{\epsilon}$) and permeability tensor

($\overleftrightarrow{\mu}$) which can be written in Cartesian coordinates in the form:

$$\overleftrightarrow{\epsilon}=\begin{pmatrix}\epsilon_\perp & 0 & 0\\ 0 & \epsilon_\perp & 0\\ 0 & 0 & \epsilon_\parallel\end{pmatrix} \tag{1a}$$

and

$$\overleftrightarrow{\mu}=\begin{pmatrix}\mu_\perp & 0 & 0\\ 0 & \mu_\perp & 0\\ 0 & 0 & \mu_\parallel\end{pmatrix}, \tag{1b}$$

where the nonzero elements of the tensor are, in general, frequency dependent. The subscript $\parallel$ ($\perp$) means the correspondent function parallel (perpendicular) to the axis of the uniaxial anisotropy.

We consider a polariton propagating parallel to the axis of the cylinder, with wave vector k and frequency ω, to write the components of the electromagnetic field as[13]

$$\mathbf{E}=[\mathbf{E_r}(\mathbf{r}),\mathbf{E}_\theta(\mathbf{r}),\mathbf{E}_z(\mathbf{r})]\mathbf{S_n}, \tag{2a}$$

and

$$\mathbf{H}=[\mathbf{H_r}(\mathbf{r}),\mathbf{H}_\theta(\mathbf{r}),\mathbf{H}_z(\mathbf{r})]\mathbf{S_n}, \tag{2b}$$

with

$$S_n=\exp[i(kz+n\theta-\omega t)], \tag{3}$$

where $\hat{\mathbf{r}}$ ($\hat{\mathbf{z}}$) is the direction perpendicular (parallel) to the axis of the cylinder, $\hat{\theta}$ is the direction defined by $\hat{\mathbf{r}}\times\hat{\mathbf{z}}$, and in Eq. (3) n is an integer since the solutions must be single value functions. Hence, from Maxwell's equations in cylindrical coordinates we find the components of the electric and magnetic field obeying the equations:

$$\frac{1}{r}(nE_z-krE_\theta)=\mu_\perp\frac{\omega}{c}H_r, \tag{4a}$$

$$\frac{dE_z}{dr}-ikE_r=-i\mu_\perp\frac{\omega}{c}H_\theta, \tag{4b}$$

$$\frac{d}{dr}(rE_\theta)-inE_r=i\mu_\parallel\frac{\omega}{c}rH_z, \tag{4c}$$

$$\epsilon_\perp\frac{\omega}{c}rE_r=krH_\theta-nH_z, \tag{4d}$$

$$i\epsilon_\perp\frac{\omega}{c}E_\theta=\frac{dH_z}{dr}-ikH_r, \tag{4e}$$

$$i\epsilon_\parallel\frac{\omega}{c}rE_z=inH_r-\frac{d}{dr}(rH_\theta), \tag{4f}$$

$$\mu_\perp\frac{d}{dr}(rH_r)+in\mu_\perp H_\theta+ikr\mu_\parallel H_z=0, \tag{4g}$$

and

$$\epsilon_\perp\frac{d}{dr}(rE_r)+in\epsilon_\perp E_\theta+ikr\epsilon_\parallel E_z=0. \tag{4h}$$

In general, Eqs. (4a)–(4g) present two independent solutions: namely, the pure electric waves (TE modes) and pure magnetic modes (TM modes), where in the TE (TM) mode the component $E_z(H_z)$ is equal to zero and cannot be separated if the wave has some angular dependence ($n\neq 0$).[10] Thus, it is easy to show that the z component $F_z=E_z$(or H_z) satisfies the equation:

$$r\frac{d}{dr}\left[r\frac{dF_z}{dr}\right]+[(\gamma r)^2-n^2]F_z=0 \tag{5}$$

with

$$\gamma^2=\begin{cases}\alpha_{in}^2=\dfrac{\mu_\parallel}{\mu_\perp}k_{\rm in}^2, & \text{TE modes}\\ \beta_{in}^2=\dfrac{\epsilon_\parallel}{\epsilon_\perp}k_{\rm in}^2, & \text{TM modes}\end{cases} \tag{6}$$

and

$$k_{\rm in}^2=\frac{\omega^2}{c^2}\epsilon_\perp\mu_\perp-k^2, \tag{7}$$

whose solutions are the Bessel functions

$$F_z=Z_n(\gamma r) \tag{8}$$

of the first type, which will be rewritten as Bessel functions of the second type when its argument is imaginary.[15]

We use Eq. (8) in Eqs. (4a)–(4g) to obtain the general solution for the components of the electric and magnetic fields, inside the cylinder ($r<a$) for the mode n, in the form:

$$E_r^{\rm in}=\left[\frac{ik}{k_{in}}\sqrt{\frac{\epsilon_\parallel}{\epsilon_\perp}}Z_n'(\beta_{\rm in}r)A_n-\frac{n\omega\mu_\perp}{crk_{\rm in}^2}Z_n(\alpha_{\rm in}r)B_n\right]S_n, \tag{9a}$$

$$E_\theta^{\rm in}=\left[-\frac{nk}{rk_{\rm in}^2}Z_n(\beta_{\rm in}r)A_n-\frac{i\omega}{ck_{\rm in}}\sqrt{\mu_\parallel\mu_\perp}Z_n'(\alpha_{\rm in}r)B_n\right]S_n, \tag{9b}$$

$$E_z^{\rm in}=[Z_n(\beta_{\rm in}r)A_n]S_n, \tag{9c}$$

and

$$H_r^{\rm in}=\left[\frac{n\omega}{crk_{\rm in}^2}\epsilon_\perp Z_n(\beta_{\rm in}r)A_n+\frac{ik}{k_{\rm in}}\sqrt{\frac{\mu_\parallel}{\mu_\perp}}Z_n'(\alpha_{in}r)B_n\right]S_n, \tag{10a}$$

$$H_\theta^{\rm in}=\left[\frac{i\omega}{ck_{\rm in}}\sqrt{\epsilon_\parallel\epsilon_\perp}Z_n'(\beta_{\rm in}r)A_n-\frac{nk}{rk_{\rm in}^2}Z_n(\alpha_{\rm in}r)B_n\right]S_n, \tag{10b}$$

$$H_z^{\rm in}=[Z_n(\alpha_{\rm in}r)B_n]S_n. \tag{10c}$$

Outside the cylinder ($r>a$) these components are given by

$$E_r^{\rm out}=\left[-\frac{ik}{k_{\rm out}}K_n'(k_{\rm out}r)C_n+\frac{n\omega\mu_0}{crk_{\rm out}^2}K_n(k_{\rm out}r)D_n\right]S_n, \tag{11a}$$

$$E_\theta^{\rm out}=\left[\frac{nk}{rk_{\rm out}^2}K_n(k_{\rm out}r)C_n+\frac{i\omega}{ck_{\rm out}}K_n'(k_{\rm out}r)D_n\right]S_n, \tag{11b}$$

$$E_z^{\rm out}=[K_n(\beta_{\rm in}r)C_n]S_n\,, \tag{11c}$$

and

$$H_r^{\rm out}=\left[-\frac{n\omega}{crk_{\rm out}^2}\epsilon_0K_n(k_{\rm out}r)C_n-\frac{ik}{k_{\rm out}}K_n'(k_{\rm out}r)B_n\right]S_n, \tag{12a}$$

$$H_\theta^{\rm out}=\left[-\frac{i\omega}{ck_{\rm out}}\epsilon_0K_n'(k_{\rm out}r)C_n+\frac{nk}{rk_{\rm out}^2}K_n(k_{\rm out}r)D_n\right]S_n\,, \tag{12b}$$

$$H_z^{\rm out}=[K_n(k_{\rm out}r)D_n]S_n\,, \tag{12c}$$

where $Z'(x)=dZ(x)/dx$, $k_{\rm out}^2=k^2-\omega^2/c^2\epsilon_\perp\mu_\perp>0$, and $H_n(x)$ is the Hankel function of order n since we are considering nonradiative modes.

The dispersion relation of polaritons propagating in the cylinder is obtained by using the usual Maxwell's boundary conditions for the fields at $r=a$ and the fact that they are finite at $r=0$ and $r=\infty$. In doing this we obtain the implicit dispersion relation for the confined and localized nonradiative modes given by

$$\left[\frac{\sqrt{\mu_\parallel\mu_\perp}}{k_{\rm in}a}\frac{Z_n'(\alpha_{\rm in}a)}{Z_n(\alpha_{\rm in}a)}+\frac{\mu_0}{k_{\rm out}a}\frac{H_n'(k_{\rm out}a)}{H_n(k_{\rm out}a)}\right]\times\left[\frac{\sqrt{\epsilon_\parallel\epsilon_\perp}}{k_{\rm in}a}\frac{Z_n'(\beta_{\rm in}a)}{Z_n(\beta_{\rm in}a)}+\frac{\epsilon_0}{k_{\rm out}a}\frac{H_n'(k_{\rm out}a)}{H_n(k_{\rm out}a)}\right]-\frac{n^2k^2}{(\omega/c)^2}\left[\frac{1}{(k_{\rm out}a)^2}+\frac{1}{(k_{\rm in}a)^2}\right]^2=0. \tag{13}$$

It should be remarked that the result presented in Eq. (13) coincides with the one obtained by Pfeiffer *et al.*[10] for the case of isotropic materials.

Since the time average of the instantaneous power-flow density[16] is given by

$$\mathbf{S}(\mathbf{r})=\frac{c}{8\pi}\,{\rm Re}\,\langle\mathbf{E}(\mathbf{r},t)\times\mathbf{H}^*(\mathbf{r},t)\rangle, \tag{14}$$

where $\langle\cdots\rangle$ represents the time average, the power flow with which we shall be concerned can be written as

$$P^{\rm tot}(q,\omega)=P^{\rm in}(q,\omega)+P^{\rm out}(q,\omega) \tag{15}$$

with

$$P^{\rm in}(q,\omega)=\int_0^a rdr\int_0^{2\pi}S_z^{\rm in}(r)d\theta \tag{16a}$$

and

$$P^{\rm out}(q,\omega)=\int_a^\infty rdr\int_0^{2\pi}S_z^{\rm out}(r)d\theta, \tag{16b}$$

since the time average of $\mathbf{S}(\mathbf{r})$ is z directed, with $S_z^{\rm in}(r)$ $[S_z^{\rm out}(r)]$ representing the time average power-flow density in the region $r\leqslant a$ $(r\geqslant a)$, and given by

$$S_z^{\rm in}(r)=\frac{c}{4\pi}\left\{\left(\frac{\omega k}{2ck_{\rm in}^2}\right)[\epsilon_\parallel[G_n'(\beta_{\rm in}r)]^2E_{0z}^2+\mu_\parallel[G_n'(\alpha_{\rm in}r)]^2|H_{0z}|^2]+\frac{n^2\omega k}{2cr^2k_{\rm in}^4}[\epsilon_\perp[G_n(\beta_{\rm in}r)]^2E_{0z}^2+\mu_\perp[G_n(\alpha_{\rm in}r)]^2|H_{0z}|^2]+\frac{in}{2rk_{\rm in}^3}\left[G_n(\alpha_{\rm in}r)G_n'(\beta_{\rm in}r)\left(\frac{\omega^2}{c^2}\mu_\perp\sqrt{\epsilon_\parallel\epsilon_\perp}+k^2\sqrt{\frac{\epsilon_\parallel}{\epsilon_\perp}}\right)+G_n'(\alpha_{\rm in}r)G_n(\beta_{\rm in}r)\times\left(\frac{\omega^2}{c^2}\epsilon_\perp\sqrt{\mu_\parallel\mu_\perp}+k^2\sqrt{\frac{\mu_|}{\mu_\perp}}\right)\right]E_{0z}H_{0z}\right\}, \tag{17}$$

and

$$S_z^{\rm out}(r)=\frac{c}{4\pi}\left\{\left(\frac{\omega k}{2ck_{\rm out}^2}[G_n'(k_{\rm out}r)]^2+\frac{n^2\omega k}{2cr^2k_{\rm out}^4}[G_n(k_{\rm out}r)]^2\right)[\epsilon_0E_{0z}^2+\mu_0|H_{0z}|^2]+\frac{in}{rk_{\rm out}^3}\left[\frac{\omega^2}{c^2}\mu_0\epsilon_0+k^2\right]G_n'(k_{\rm out}r)G_n(k_{\rm out}r)E_{0z}H_{0z}\right\}, \tag{18}$$

with

$$G_n(\gamma_{\rm in}r)=\frac{Z_n(\gamma_{\rm in}r)}{Z_n(\gamma_{\rm in}a)}, \tag{19a}$$

for fields inside the cylinder

$$G_n(k_{\rm out}r)=\frac{K_n(k_{\rm out}r)}{K_n(k_{\rm out}a)}, \tag{19b}$$

for fields outside the cylinder, and

$$E_{0z}=K_n(k_{\rm out}a)A_n\,, \tag{20a}$$

$$H_{0z}=\pm i\frac{T_n}{U_n}K_n(k_{\rm out}a)C_n \tag{20b}$$

with

$$T_n=\frac{nk}{a}\left(\frac{1}{k_{\rm out}^2}\pm\frac{1}{k_{\rm in}^2}\right), \tag{21a}$$

$$U_n=\frac{\omega}{c}\left[\frac{\sqrt{\mu_{|}\mu_{\perp}}}{k_{\rm in}}G_n^{'}(\alpha_{\rm in}a)\pm\frac{\mu_0}{k_{\rm out}}G_n^{'}(k_{\rm out}a)\right], \tag{21b}$$

where the signal $+$ $(-)$ in Eqs. (21a) and (21b) is associated with the volume (surface) modes and the derivatives in these equations are taken with respect to the argument.

In order to obtain the energy per unit length of the cylinder we must first calculate the energy density, which for the dispersive medium is in general[16]

$$U=\frac{1}{8\pi}\left[\frac{d}{d\omega}(\omega\vec{\epsilon})\mathbf{E}\cdot\mathbf{E}^{*}+\frac{d}{d\omega}(\omega\vec{\mu})\mathbf{H}\cdot\mathbf{H}^{*}\right], \tag{22}$$

which in our case can be separated into two terms $U^{\rm in}(r)$ $[U^{\rm out}(r)]$ representing the energy density in the region $r\leqslant a$ $(r\geqslant a)$. For the energy density $U^{\rm in}(r)$, we obtain

$$U^{\rm in}(r)=\frac{1}{16\pi}\left[\epsilon_{\perp}\{|E_r^{\rm in}|^2+|E_\theta^{\rm in}|^2\}+\left(\mu_{\perp}+\omega\frac{d\mu_{\perp}}{d\omega}\right)\{|H_r^{\rm in}|^2+|H_\theta^{\rm in}|^2\}+\epsilon_{\|}|E_z^{\rm in}|^2+\mu_{\|}|H_z^{\rm in}|^2\right], \tag{23}$$

with

$$(E_r^{\rm in})^2=\frac{n^2\omega^2}{c^2r^2k_{\rm in}^4}\mu_{\perp}{}^2[G_n(\alpha_{\rm in}r)]^2|H_{0z}|^2+\frac{k^2\epsilon_{\|}}{k_{\rm in}^2\epsilon_{\perp}}[G_n^{'}(\beta_{\rm in}r)]^2E_{0z}^2+\frac{2ink\omega}{crk_{\rm in}^3}\mu_{\perp}\sqrt{\frac{\epsilon_{\|}}{\epsilon_{\perp}}}G_n(\alpha_{\rm in}r)G_n^{'}(\beta_{\rm in}r)E_{0z}H_{0z}\,, \tag{24a}$$

$$(E_\theta^{\rm in})^2=\frac{\omega^2}{c^2k_{\rm in}^2}\mu_{\|}\mu_{\perp}[G_n^{'}(\alpha_{\rm in}r)]^2|H_{0z}|^2+\frac{n^2k^2}{r^2k_{in}^4}[G_n(\beta_{\rm in}r)]^2E_{0z}^2+\frac{2ink\omega}{crk_{\rm in}^3}\sqrt{\mu_{\|}\mu_{\perp}}G_n^{'}(\alpha_{\rm in}r)G_n(\beta_{\rm in}r)E_{0z}H_{0z}\,, \tag{24b}$$

and

$$\left(E_z^{\rm in}\right)^2=Z_n(\beta_{\rm in}r)^2E_{0z}^2 \tag{24c}$$

for the components of the electric field, and

$$(H_r^{\rm in})^2=\frac{n^2\omega^2}{c^2r^2k_{\rm in}^4}\epsilon_{\perp}{}^2[G_n(\beta_{\rm in}r)]^2E_{0z}^2+\frac{k^2\mu_{\|}}{k_{\rm in}^2\mu_{\perp}}[G_n^{'}(\alpha_{\rm in}r)]^2|H_{0z}|^2+\frac{2ink\omega}{crk_{\rm in}^3}\epsilon_{\perp}\sqrt{\frac{\mu_{\|}}{\mu_{\perp}}}G_n^{'}(\alpha_{\rm in}r)G_n(\beta_{\rm in}r)E_{0z}H_{0z}\,, \tag{25a}$$

$$(H_\theta^{\rm in})^2=\frac{\omega^2}{c^2k_{\rm in}^2}\epsilon_{\|}\epsilon_{\perp}[G_n^{'}(\beta_{\rm in}r)]^2E_{0z}^2+\frac{n^2k^2}{r^2k_{\rm in}^4}[G_n(\alpha_{\rm in}r)]^2|H_{0z}|^2+\frac{2ink\omega}{crk_{\rm in}^3}\sqrt{\epsilon_{\|}\epsilon_{\perp}}G_n(\alpha_{\rm in}r)G_n^{'}(\beta_{\rm in}r)E_{0z}H_{0z}\,, \tag{25b}$$

and

$$(H_z^{\rm in})^2=[G_n(\alpha_{\rm in}r)]^2H_{0z}^2 \tag{25c}$$

for the components of the magnetic field. For the energy density $U^{\rm out}(r)$ we obtain

$$U^{\rm out}=\frac{1}{16\pi}[\epsilon_0|E_n^{\rm out}|^2+\mu_0|H_n^{\rm out}|^2], \tag{26}$$

where

$$|E_n^{\rm out}|^2=(E_r^{\rm out})^2+(E_\theta^{\rm out})^2+(E_z^{\rm out})^2, \tag{27a}$$

$$|H_n^{\rm out}|^2=(H_r^{\rm out})^2+(H_\theta^{\rm out})^2+(H_z^{\rm out})^2 \tag{27b}$$

with

$$(E_r^{\rm out})^2=\frac{\omega^2}{c^2r^2k_{\rm out}^4}\mu_0{}^2[G_n(k_{\rm out}r)]^2|H_{0z}|^2+\frac{k^2}{k_{\rm out}^2}[G_n'(k_{\rm out}r)]^2E_{0z}^2+\frac{2ik\omega}{crk_{\rm out}^3}\mu_0G_n(k_{\rm out}r)G_n'(k_{\rm out}r)E_{0z}H_{0z}, \tag{28a}$$

$$(E_\theta^{\rm out})^2=\frac{\omega^2}{c^2k_{\rm out}^2}\mu_0{}^2[G_n'(k_{\rm out}r)]^2|H_{0z}|^2+\frac{k^2}{r^2k_{\rm out}^4}[G_n(k_{\rm out}r)]^2E_{0z}^2+\frac{2ik\omega}{crk_{\rm out}^3}\mu_0G_n'(k_{\rm out}r)G_n(k_{\rm out}r)E_{0z}H_{0z}, \tag{28b}$$

and

$$(E_z^{\rm out})^2=[G_n(k_{\rm out}r)]^2E_{0z}^2 \tag{28c}$$

for the components of the electric field, and

$$(H_r^{\rm out})^2=\frac{n^2\omega^2}{c^2r^2k_{\rm out}^4}\epsilon_0{}^2[G_n(k_{\rm out}r)]^2E_{0z}{}^2+\frac{k^2}{k_{\rm out}^2}[G_n'(k_{\rm out}r)]^2|H_{0z}|^2+\frac{2ik\omega}{crk_{\rm out}^3}\epsilon_0G_n'(k_{\rm out}r)G_n(k_{\rm out}r)E_{0z}H_{0z}, \tag{29a}$$

$$(H_\theta^{\rm out})^2=\frac{\omega^2}{c^2k_{\rm out}^2}\epsilon_0{}^2[G_n'(k_{\rm out}r)]^2E_{0z}{}^2+\frac{k^2}{r^2k_{\rm out}^4}[G_n(k_{\rm in}r)]^2|H_{0z}|^2+\frac{2ik\omega}{crk_{\rm out}^3}\epsilon_0G_n(k_{\rm out}r)G_n'(k_{\rm out}r)E_{0z}H_{0z}, \tag{29b}$$

and

$$(H_z^{\rm out})^2=[G_n(k_{\rm out}r)]^2|H_{0z}|^2 \tag{29c}$$

for the components of the magnetic field.

The energy per unit length of the cylinder $Y^{\rm tot}(q,\omega)$ is obtained by integrating the energy density, and is given by

$$Y^{\rm tot}(q,\omega)=Y^{\rm in}(q,\omega)+Y^{\rm out}(q,\omega) \tag{30}$$

with

$$Y^{\rm in}(q,\omega)=\int_0^a rdr\int_0^{2\pi}U^{\rm in}(r)d\theta \tag{31a}$$

and

$$Y^{\rm out}(q,\omega)=\int_a^\infty rdr\int_0^{2\pi}U^{\rm out}(r)d\theta. \tag{31b}$$

Finally, the energy transport velocity[10] that is equal to the group velocity, is given by

$$v_E=\frac{P^{\rm tot}(q,\omega)}{Y^{\rm tot}(q,\omega)}. \tag{32}$$

III. NUMERICAL RESULTS

The analytical results displayed in Sec. II can be used to obtain a complete description of polaritons propagating in any anisotropic cylinder, provided its dielectric constant and magnetic permeability can be written in the form given by Eqs. (1a) and (1b). In order to have numerical results, we choose the uniaxial Heisenberg antiferromagnet MnF_2 as the anisotropic material. This material is a prototype of an anisotropic magnetic material and all parameters necessary to describe it are very well known.[3] In the following, we present the numerical results for the dispersion relation of the volume and surface modes, power-flow density, energy density, and the energy velocity considering the MnF_2, immerse in vacuum ($\epsilon_0=1.0,\mu_0=1.0$). This material is characterized by the dielectric tensor, Eq. (1a), with $\epsilon_\parallel=4.0$, $\epsilon_\perp=5.5$ and the permeability tensor by Eq. (1b), with the nonzero components of the magnetic permeability tensor given by $\mu_\perp(\omega)=1+\Omega_s^2/(\Omega_0^2-\omega^2)$ and $\mu_\parallel=1.0$, where $\Omega_0=\gamma(2H_EH_A+H_A^2)^{1/2}$ is the antiferromagnetic resonance frequency, $\Omega_S=\gamma(8\pi H_AM_S)^{1/2}$ with $\gamma=1.8\times10^7$ rad/G denoting the gyromagnetic factor, $H_A=7.85$ kG is the anisotropy field, $H_E=550$ kG the exchange field, and $M_S=0.6$ kG the saturation magnetization of each sublattice.[3]

We solve Eq. (13) numerically to obtain the dispersion curves of polaritons associated with confined and localized modes. The confined modes are characterized by the fact that $\alpha_{\rm in}$ and $\beta_{\rm in}$ in Eq. (13) are both real numbers, while the surface modes have these parameters imaginary. We should mention that modes with $n=0$ are not influenced by the curvature of the cylinder and consequently have their behavior similar to the planar geometry. In Fig. 1 we present the dispersion relation of confined and surface (localized) modes as a function of the wave vector of the polariton, for a cylinder of radius (a) $a=0.5$ mm and (b) 2.0 mm with $n=1$. Although the cylinder with $a=0.5$ mm presents a confined mode in the region $\omega<\Omega_0$, its frequency is extremely close to the resonance line ($\omega=\Omega_0$). For this reason only the confined modes for the cylinder with $a=2.0$ mm which are propagating with $\omega<\Omega_0$ were plotted. The cylinder with radius $a=2.0$ mm presents a larger number of branches compared with the one with $a=0.5$ mm, showing that the number of branches of confined modes increases with the cylinder radius. Particularly, for an isotropic dielectric material with a cylindrical geometry Pfeiffer *et al.*[10] observed localized modes in the region $\epsilon<0$. However, for the uniaxial

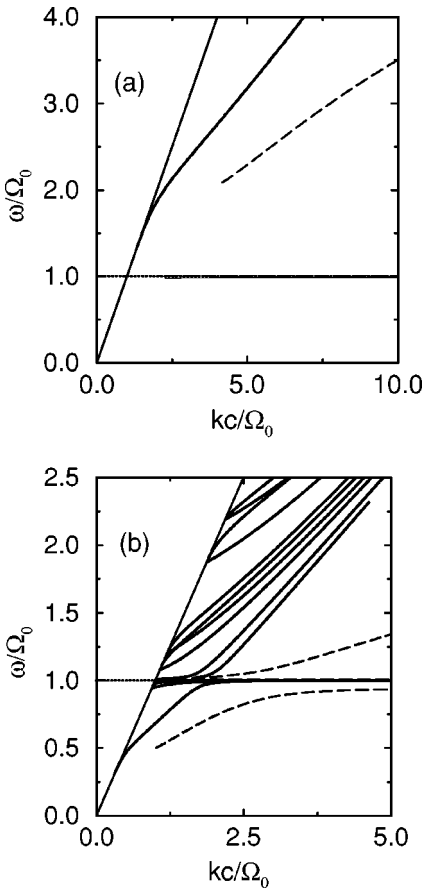

FIG. 1. Dispersion relation of confined (solid curve) and localized (dashed curve) modes of the polariton as a function of the wave vector, for a cylinder with radius (a) $a=0.5$ mm and (b) $a=2.0$ mm.

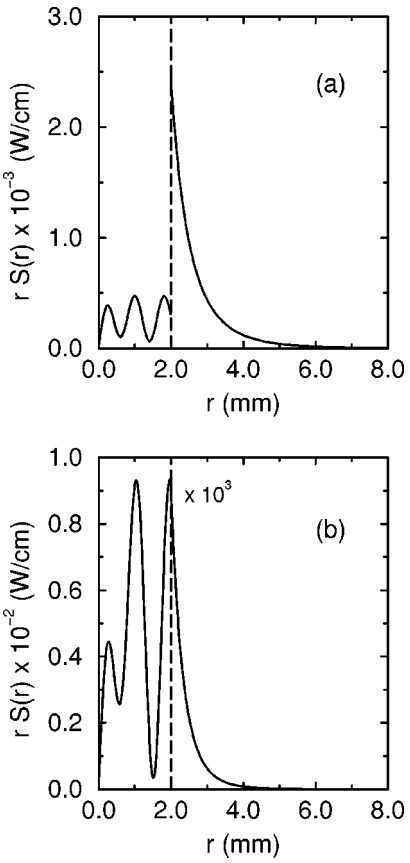

FIG. 2. The function $rS_z(r)$ for polaritons on confined modes with $n=1$ as a function of the distance from the cylinder axis, for a cylinder of radius $a=2.0$ mm, for the eighth (a) and seventh (b) branches with frequency $\omega=2.13\Omega_0$, corresponding to $k=2.31\Omega_0/c$ and $k=2.75\Omega_0/c$, respectively.

Heisenberg antiferromagnet studied here, in the region where $\mu_\perp<0$ (which corresponds to the frequency region $\Omega_0^2<\omega^2<\Omega_0^2+\Omega_S^2$), we observed modes with mixed character, i.e., the solutions present oscillating and decay character simultaneously. Since this frequency region is very narrow for this material, we will not discuss this case. Considering $n=1$, we observed that for both cylinders mentioned above, there are localized modes in the frequency region where $\mu_\perp>0$ corresponding to frequencies $\omega^2>\Omega_0^2+\Omega_S^2$ or $\omega<\Omega_0$. The localized mode which appears in the region where $\omega<\Omega_0$ in the cylinder of radius, $a=0.5$ mm has its frequency almost constant and equal to the resonance frequency Ω_0, see Fig. 1(a). For the cylinder with radius $a=2.0$ mm, Fig. 1(b), the localized modes appear for smaller values of the wave vector compared to the one with radius $a=0.5$ mm. Differently from the confined modes, the number of localized modes does not change with the cylinder radius.

The knowledge of the dispersion relation does not provide all the information necessary to analyze the propagation of polaritons. For this reason we now present the results for the time-average power flux, energy density, integrate power flow, energy per unit length, and finally energy transport velocity. For the polariton propagating in the confined mode, the power flow inside the cylinder oscillates, while outside it decays. This behavior comes from the fact that the fields that describe this mode are Bessel functions of the first type inside and Bessel functions of the second type outside the cylinder. The discontinuity of the power flow at the interface $r=a$ for both modes is a consequence of discontinuity of the fields at this interface. To analyze the power flow, we first plot in Fig. 2 the function $rS_z(r)$ for polaritons, propagating with the same frequency but in two different branches of confined modes, as a function of the distance from the cylinder axis, for a cylinder of radius $a=2.0$ mm, with $n=1$ and in the region of frequency $\omega^2>\Omega_0^2+\Omega_S^2$. We choose the polaritons in the eighth and seventh branches above the resonance line, which have frequency $\omega=2.13\ \Omega_0$, corresponding to $k=2.31\ \Omega_0/c$ [Fig. 2(a)] and $k=2.75\ \Omega_0/c$ [Fig. 2(b)], respectively. In Fig. 2(a) we observed that the power flow inside the cylinder is smaller than the power flow outside the cylinder, while in Fig. 2(b) the intensity of the power flow inside the cylinder is considerable larger (three orders of magnitude) compared with its intensity outside the cylinder. In fact we observed that, for confined modes in the region $\omega^2>\Omega_0^2+\Omega_S^2$, where the second derivative of the dispersion curve is negative, such as in the eight branch, the power flow inside the cylinder is smaller than outside, while an opposite behavior is observed in the branches on which the second derivative of the dispersion curve is positive. In a cylinder of $a=0.5$ mm the confined mode with frequency

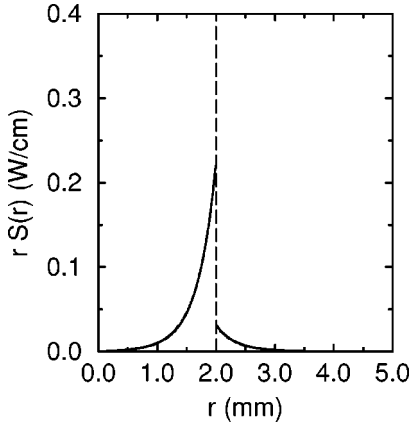

FIG. 3. The function $rS_z(r)$ for a polariton on a localized mode with $n=1$ as a function of the distance from the cylinder axis, for a cylinder of radius $a=2.0$ mm, corresponding to a frequency $\omega=1.04\Omega_0$.

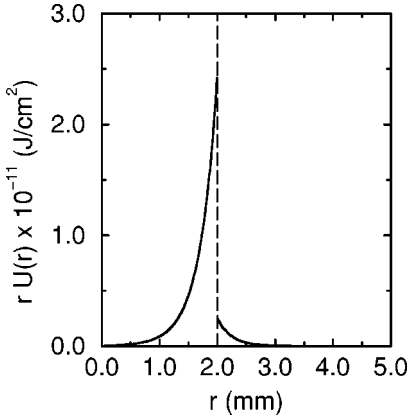

FIG. 5. The function $rU(r)$ for a polariton in the localized mode with $n=1$ as a function of the distance from the cylinder axis, for a cylinder of radius $a=2.0$ mm, corresponding to a frequency $\omega=1.04\Omega_0$.

above $\sqrt{\Omega_0^2+\Omega_S^2}$ also presents a second derivative of the dispersion curve negative, and we observed that the power flow inside the cylinder is also smaller than outside, representing an analogous behavior to the one observed for the power flow of the confined mode shown in Fig. 2(a). However, we observed that confined modes with frequency below the resonance, have the second derivative of the dispersion curve negative, but the intensity of the power flow inside the cylinder is greater than outside.

For localized modes, in Fig. 3 we show the function $rS_z(r)$ as a function of the distance from the cylinder axis, for $a=2.0$ mm, with $n=1$ and in the region of frequency $\omega^2>\Omega_0^2+\Omega_S^2$. As can be seen, the power flow inside is considerable larger than outside the cylinder. This fact is also observed for the mode below the resonance frequency. Particularly, for a cylinder of radius $a=0.5$ mm, the power flux inside it is one order of magnitude larger than the power flow outside the cylinder. This behavior is different from the one observed by Khosravi *et al.*[11] in localized modes of a cylinder with isotropic dielectric material with $n=1$, where the intensity of the power flow is of the same order of magnitude. We observed that the difference in magnitude, between the power flow inside and outside the cylinder, decreases with the cylinder radius.

To analyze the energy density of the polariton propagating in a cylinder we show in Figs. 4(a) and 4(b), the function $rU(r)$ as a function of the distance from the cylinder axis, for a cylinder of radius $a=2.0$ mm, corresponding to the same modes considered in Figs. 2(a) and 2(b), respectively. In both cases we observe that the energy density is greater

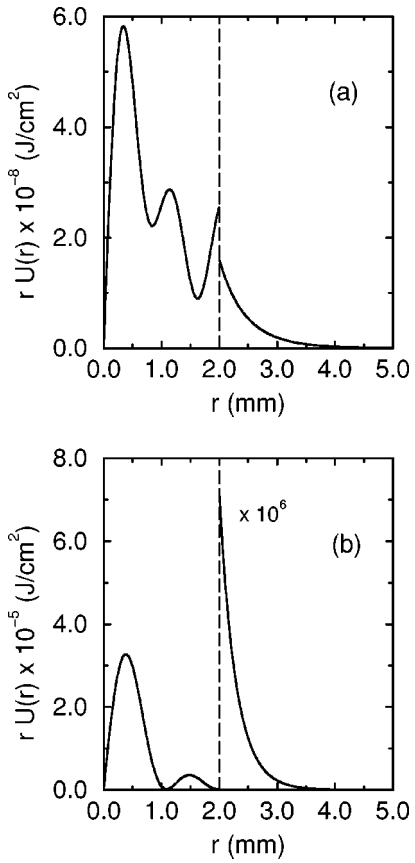

FIG. 4. The function $rU(r)$ for polaritons on confined modes with $n=1$ as a function of the distance from the cylinder axis, for a cylinder of radius $a=2.0$ mm, for the eighth (a) and seventh (b) branches with frequency $\omega=2.13\Omega_0$, corresponding to $k=2.31\Omega_0/c$ and $k=2.75\Omega_0/c$, respectively.

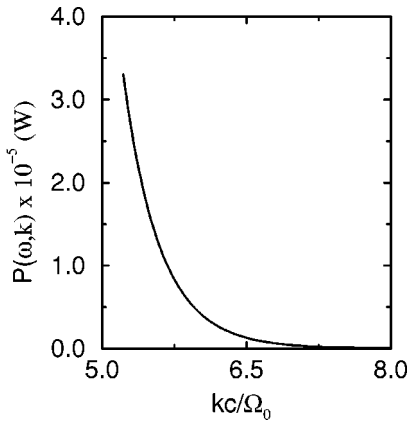

FIG. 6. The integrated power flow of the localized mode in the region $\omega>\sqrt{\Omega_0^2+\Omega_S^2}$ as a function of the wave vector, for a cylinder of radius $a=0.5$ mm and with $n=1$.

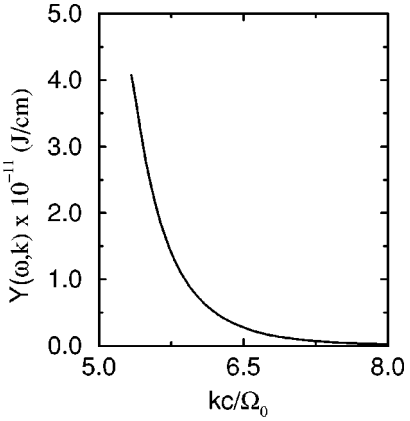

FIG. 7. The energy per unit length of the localized mode in the region $\omega > \sqrt{\Omega_0^2 + \Omega_S^2}$ as a function of the wave vector, for a cylinder of radius $a = 0.5$ mm and with $n = 1$.

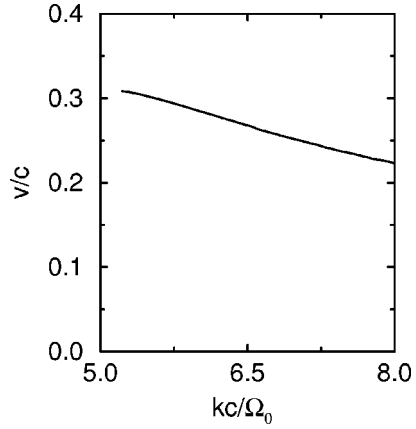

FIG. 8. The energy velocity of the localized mode in the region $\omega > \sqrt{\Omega_0^2 + \Omega_S^2}$ as a function of the wave vector, for a cylinder of radius $a = 0.5$ mm and with $n = 1$.

inside the cylinder than it is outside the cylinder, independent of the signal of the second derivative of the dispersion curve. As can be seen in Fig. 5, the energy density has a similar behavior for the localized mode presented in Fig. 3, but the difference between the values inside and outside is only one order of magnitude.

For the results of the integrated power flow Eq. (15) and the energy per unit length Eq. (30) we will restrict our attention to localized modes, since they can be compared with those obtained by Khosravi *et al.*[11] in a cylinder with isotropic dielectric. In Figs. 6 and 7 we present the integrated power flow and energy per unit length of the localized mode in the region $\omega^2 > \Omega_0^2 + \Omega_S^2$ as a function of the wave vector, for a cylinder of radius $a = 0.5$ mm and with $n = 1$. As can be seen, the integrated power flow and the energy per unit length decreases with the wave vector and are always positive. We should mention that this behavior is also observed for the confined modes studied here. This characteristic is not observed in an isotropic dielectric cylinder[11] where the integrated power flow is negative in the region where the slope of the corresponding dispersion curve is negative. For the anisotropic material considered and the modes investigated, the slope of the dispersion curves did not change signal and consequently it could be expected that the integrated power flow and energy per unit length had the same signal. These facts show consistency in Fig. 8, where we present the energy transport velocity of the localized modes presented in Figs. 6 and 7, given by Eq. (32), which is in qualitative agreement with the group velocity found as the slope of the corresponding dispersion curve.

IV. CONCLUSIONS

We have investigated the properties of polaritons propagating in an anisotropic material with a cylindrical geometry. The analytical equations obtained are general and the results can be used to have a complete description of polaritons in cylindrical geometry. It should be remarked that the result for an isotropic cylinder can be obtained as a particular case. We choose the uniaxial Heisenberg antiferromagnet MnF_2 to display numerical results of the dispersion curves of confined and localized modes, power-flow density, energy density, and the energy transport velocity. As discussed in Sec. III, the many branches of confined and localized modes present different behaviors of propagation and remarkable variations on the intensities of electromagnetic fields, inside and outside the cylinder. In isotropic dielectric materials with the same geometry considered here and a fixed radius, the different modes are restricted to regions of negative values of dielectric function. Considering a cylinder with the same radius and an anisotropic material we observed a much larger range of frequencies on which polaritons can propagate. The existence of damping was not considered but consists in an important point to be studied in order to analyze the decay of different modes. This subject is now under consideration.

Finally, we should say that we have applied our analytical calculations to study the behavior of polaritons in a uniaxial Heisenberg antiferromagnet cylinder but we do not expect qualitative changes for propagation of these modes in a different anisotropic medium with the same geometry.

ACKNOWLEDGMENTS

G.A.F. is partially supported by the Brazilian Agencies, Fundação Cearense de Amparo à Pesquisa (FUNCAP), Brazilian National Research Council (CNPq) and The Ministry of Planning (FINEP), and N.S.A. is partially supported by the Brazilian National Research Council (CNPq).

*Electronic address: gil@fisica.ufc.br

[1] A. A. Maradudin, *Electromagnetic Surface Excitations* , edited by R. F. Wallis and G. I. Stegeman (Springer-Verlag, Berlin, 1986).
[2] E. L. Albuquerque and M. G. Cottam, Phys. Rep. **233**, 67 (1993).
[3] D. L. Mills and E. Burstein, Rep. Prog. Phys. **37**, 817 (1974).
[4] R. E. Camley and D. L. Mills, Phys. Rev. B **26**, 1280 (1982).
[5] V. D. Buchel'nikov and V. G. Shavrov, Sov. Phys. JETP **82**, 380 (1996).

[6] R. L. Stamps and R. E. Camley, Phys. Rev. B **54**, 15 200 (1996).
[7] M. R. F. Jensen, T. J. Parker, Kamsul Abraha, and D. R. Tilley, Phys. Rev. Lett. **75**, 3756 (1995).
[8] A. Madrazo and M. Nieto-Vesperinas, J. Opt. Soc. Am. A **13**, 785 (1996); **12**, 1298 (1995).
[9] J. P. Valle, F. Gonzales, and F. Moreno, Appl. Opt. **33**, 512 (1994).
[10] C. A. Pfeiffer, E. N. Economou, and K. L. Ngai, Phys. Rev. B **10**, 3038 (1974).
[11] H. Khosravi, R. Tilley, and R. Loudon, J. Opt. Soc. Am. A **8**, 112 (1991).
[12] G. C. Aers, A. D. Boardman, and B. V. Paranjape, J. Phys. F **10**, 53 (1980).
[13] E. F. Vasconcelos, N. T. Oliveira, G. A. Farias, and N. S. Almeida, Phys. Rev. B **44**, 12 621 (1991).
[14] N. S. Almeida, G. A. Farias, N. T. Oliveira, and E. F. Vasconcelos, Phys. Rev. B **48**, 9839 (1993).
[15] M. Abramowitz and L. A. Stegun, *Handbook of Mathematical Functions* (Dover, New York, 1965).
[16] L. D. Landau and E. M. Lifshitz, *Electrodynamics of Continuous Media* (Pergamon, Oxford, 1971).